Int J Adv Manuf Technol (2013) 68:701–709
DOI 10.1007/s00170-013-4792-5

ORIGINAL ARTICLE

Identification of instantaneous cutting force coefficients using surface error

Baosheng Wang · Hongyan Hao · Mulan Wang · Junming Hou · Yong Feng

Received: 13 June 2012 / Accepted: 21 January 2013 / Published online: 6 February 2013

Abstract Cutting force coefficients are the key factors for efficient and accurate prediction of instantaneous milling force. To calibrate the coefficients, this paper presents an instantaneous milling force model including runout and cutter deformation. Also, forming of surface error is analyzed, and a surface error model considering runout is proposed. Using surface errors of two experiments completed with the same cutting conditions but different axial depth only, cutter deformation is obtained. Then, a new approach for the determination of instantaneous cutting force coefficients is provided. The method can eliminate influences of the other factors except cutter deformation and runout. A series of experiments are designed, and the results are used to identify the parameters. With the evaluated coefficients and runout parameters, the instantaneous milling force and surface error are predicted. A good agreement between predicted results and experimental results is achieved, which shows that the method is efficient, and effect of runout on surface error is not negligible.

Keywords Instantaneous cutting force coefficients · Identification · Surface error · Runout · Deformation

B. Wang (✉) · H. Hao
School of Materials Engineering, Nanjing Institute of Technology, No.1 Hongjing Street,
Nanjing 211167 Jiangsu, China
e-mail: wbaosh@163.com

M. Wang · J. Hou · Y. Feng
Jiangsu Key Laboratory of Advanced Numerical Control Technology, No.1 Hongjing Street,
Nanjing 211167 Jiangsu, China

1 Introduction

Precise prediction of milling force is essential for improving the processing efficiency, predicting the workpiece deformation and wearing of cutter, and reducing the shape error and surface roughness. Therefore, it is necessary to pay more attention to milling force. To predict the milling force with mechanistic model, the cutting force coefficients must be estimated at first. Despite the development of many versions of mechanistic models, milling force prediction still relies on the cutting force coefficients defined from empirical data.

Traditionally, the calibration of the cutting force coefficients is performed by measuring the cutting force. There exist two typical categories of cutting force coefficients calibrating methods according to whether the size effect of instantaneous chip thickness is considered. In the first one, the size effect is ignored. Cutting force coefficients are taken as constants or exponential of average chip thickness, which are called average cutting force coefficients and depend on the cutter geometry, cutting conditions, insert grade and workpiece material properties, and calibrated based on average cutting force [1–4]. Based on the method, Kang [5] and Liu [6] expressed the coefficients as quadratic polynomial functions of spindle speed, feed rate, axial depth, and radial depth using orthogonal test and regression analysis. The method is simple. However, it will decrease the accuracy of predicted instantaneous milling forces because the size effect of the chip thickness is largely neglected. Also, it requires a series of experiments to calibrate cutting force coefficients.

In the second method, many researchers take into consideration the size effect of the chip thickness in the cutting force coefficients model to meet the demand for more

accurate milling force prediction and express the cutting force coefficients as exponential function of instantaneous chip thickness, that is, instantaneous cutting force coefficients [7–9]. Bhattacharyya [10] proposed a method to identify instantaneous cutting force coefficients using average milling forces with multiple experiments. Wan [11, 12] calibrated the instantaneous cutting force coefficients using nominal milling forces which are extracted from experimental results with one experiment. Riviere-Lorphevre [13] proposed an identification algorithm for cutting force coefficients taking radial runout into account.

All contributions mentioned above are based on the measured milling forces, which obtained with special and expensive force meter. Franco [14] proposed a numerical model for predicting the surface profile and surface roughness in face milling operations as a function of feed, cutting tool geometry, and tool errors. Salgado [15] investigated the stiffness and cutting force-induced deflection of end-milling system. Furthermore, the machined surface error was analyzed. Siller [16] studied the impact of a special carbide tool design on the process viability of the face milling in terms of surface quality and tool life, and presented a method for representing relation between tool wear morphology and surface roughness. Kim [17] and Xu[18] presented methods to calibrate cutting force coefficients with surface error of workpiece on the assumption that the error is deduced by cutter deformation completely. Dotcheva [19] neglected the effect of the runout to the surface error, proposed a method to obtain the cutter deformation form surface error, and calibrate instantaneous cutting force coefficients.

This paper presents a new approach to calibrate the instantaneous cutting force coefficients. Firstly, a surface error model considering runout is proposed. The cutter deformation is separated from the surface error by experimentation. Secondly, the cutting force coefficients are identified with the help of the cutter deformation obtained above. The advantage of the proposed approach lies in that the calibration can eliminate influences of the other factors except cutter deformation and runout. Besides, a comparative study between predicted results and experimental results is made to validate the proposed method.

2 Mechanistic milling force model

Based on the work of Wan [11], the tool is discretized along the axis into segments. The tangential $dF_{ti,j}(\varphi)$ and radial $dF_{ri,j}(\varphi)$ cutting force components acting on jth element of ith flute are given by

$$\begin{cases} dF_{ti,j}(\varphi) = K_t\big(h_{i,j}(\varphi)\big)h_{i,j}(\varphi)dz \\ dF_{ri,j}(\varphi) = K_r\big(h_{i,j}(\varphi)\big)h_{i,j}(\varphi)dz \end{cases} \quad (1)$$

Where, φ is the angular position of the tool. dz is the axial length of discrete segment. $h_{i,j}(\varphi)$ is the instantaneous chip thickness. $K_t(h_{i,j}(\varphi))$ and $K_r(h_{i,j}(\varphi))$ represent the tangential and radial cutting force coefficients.

The relationships between the cutting force coefficients and the instantaneous chip thickness are expressed as

$$\begin{cases} K_t(h) = T_0 h^{T_1} \\ K_r(h) = R_0 h^{R_1} \end{cases} \quad (2)$$

Where, T_0, T_1, R_0, and R_1 are constants for a given combination of tool and workpiece material.

During milling process, when cutter runout and cutter deformation occur, the cutter axis will shift from its nominal position, and the cutting path will deviate from the nominal path. Consequently, the instantaneous chip thickness of the segment (i, j) will be calculated by the following equation.

$$h_{i,j}(\varphi) = m_i f_z \sin\theta_{i,j}(\varphi) + R_{i,j}(\varphi) - R_{i-m_i,j}(\varphi) \quad (3)$$

Where, f_z denotes the feed per tooth. m_i is a number that indicates the current tooth is removing the material left by the previous tooth. $\theta_{i,j}(\varphi)$ and $R_{i,j}(\varphi)$ are referred to as the instantaneous angular position and the instantaneous actual cutting radius of the segment (i, j).

Figure 1 shows the radial runout of the end-milling process [7]. ρ denotes the runout offset. λ is the location angle defined as the clockwise angle between offset direction and the nearest tooth tip in the bottom of cutting tool.

Figure 2 shows the cutter deformation simplified as piecewise cantilever beam. In end milling, considering the axial milling force is small and axial stiffness of cutter is large, the axial cutter deformation is neglected. To simplify the analysis, the cutting forces acting on the cutting edge segment are equivalent to concentrated forces. The points of the forces can be expressed as

$$\begin{cases} Z_x(\varphi) = L - \dfrac{\sum_{i=1}^{N}\sum_{j=1}^{M} dF_{xi,j}(\varphi)\big(L - z_{i,j}\big)}{F_x(\varphi)} \\ Z_y(\varphi) = L - \dfrac{\sum_{i=1}^{N}\sum_{j=1}^{M} dF_{yi,j}(\varphi)\big(L - z_{i,j}\big)}{F_y(\varphi)} \end{cases} \quad (4)$$

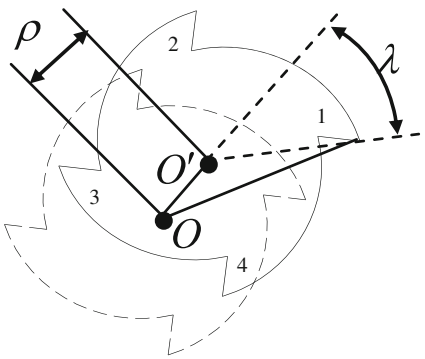

Fig. 1 Cutter runout and related parameters

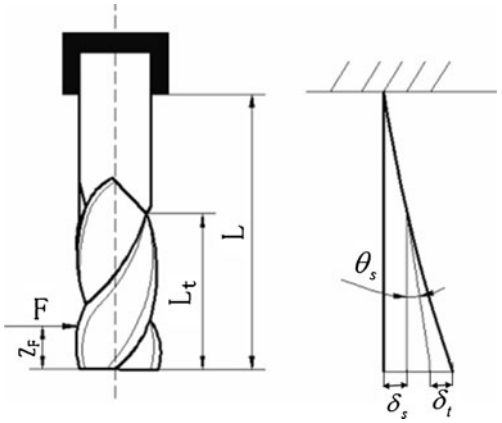

Fig. 2 Cutter deformation

Where, $Z_x(\varphi)$ and $Z_y(\varphi)$ are distances between points of simplified concentrated forces and cutter bottom. $z_{i,j}$ denotes distance between segment (i,j) and cutter bottom. L is overhang length. $F_x(\varphi)$ and $F_y(\varphi)$ are X and Y components of simplified concentrated forces. $dF_{xi,j}(\varphi)$ and $dF_{xi,j}(\varphi)$ are X and Y components of cutting forces acting on the segment (i, j). N is the number of tooth. M is the number of segment for each tooth.

As shown in Fig. 2, the total cutter deformation consists of arbor deformation and deflection of fluted part. So, the deformation of segment can be defined as

$$\begin{cases} \delta_{ct}(z_{i,j}) = \delta_s + \theta_s(z_{i,j}) + \delta_t(z_{i,j}) \\ \delta_s = \frac{F}{6EI_s}\left[-(L-L_t)^3 + 3(L-L_t)^2(L-Z_F)\right] \\ \delta_t(z_{i,j}) = \frac{F}{6EI_t}\left[\langle Z_F - z_{i,j}\rangle^3 - (L_t - z_{i,j})^3 + 3(L_t - z_{i,j})^2(L_t - Z_F)\right] \\ \theta_s(z_{i,j}) = \frac{F}{2EI_s}\left[-(L-L_t)^2 + 2(L-L_t)(L-Z_F)\right](L_t - z_{i,j}) \end{cases} \tag{5}$$

Where, $\delta_{ct}(z_{i,j})$ is the total deflection at $z_{i,j}$. δ_s is the deflection due to the deformation of cutter arbor. $\theta_s(z_{i,j})$ is the deviation due to deflection angle of cutter arbor.

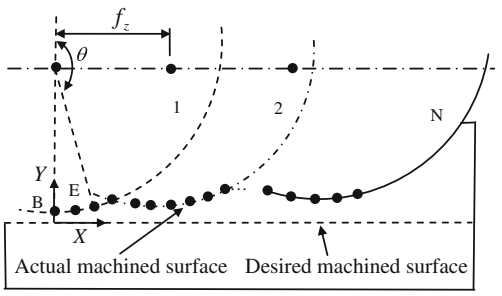

Fig. 3 Formation of surface error

$\delta_t(z_{i,j})$ is the deformation of fluted part of the cutter. Z_F denotes distance between simplified concentrated forces and cutter bottom. L_t is the length of the fluted part. I_s and I_t are the moments of inertia for the arbor and fluted part. E is Young's modulus of elasticity. $\langle\rangle$ is a window function.

With Eqs. (4) and (5), the instantaneous deformations $\delta_{xi,j}(\varphi)$ and $\delta_{yi,j}(\varphi)$ of cutter at (i, j) can be calculated. So, considering the cutter runout and deformation, the instantaneous actual cutting radius of the segment can be presented as

$$R_{i,j}(\varphi) = \frac{D}{2} + \rho\cos\left(\lambda - \frac{2z_{i,j}\tan\beta}{D} - \frac{2\pi(i-1)}{N}\right) + \delta_{xi,j}(\varphi)\sin\theta_{i,j}(\varphi) + \delta_{yi,j}(\varphi)\cos\theta_{i,j}(\varphi) \tag{6}$$

Where, D and β are the diameter and helix angle of the cutter.

Subsequently, the total milling force components at any angular position φ can be evaluated by summing the forces acting on all the flutes and segments.

$$\begin{cases} F_x(\varphi) = \sum_{i=1}^{N}\sum_{j=1}^{M}\left[-K_t(h_{i,j}(\varphi))\cos\theta_{i,j}(\varphi) - K_r(h_{i,j}(\varphi))\sin\theta_{i,j}(\varphi)\right]h_{i,j}(\varphi)dz \\ F_y(\varphi) = \sum_{i=1}^{N}\sum_{j=1}^{M}\left[K_t(h_{i,j}(\varphi))\sin\theta_{i,j}(\varphi) - K_r(h_{i,j}(\varphi))\cos\theta_{i,j}(\varphi)\right]h_{i,j}(\varphi)dz \end{cases} \tag{7}$$

3 Estimation of cutter deformation

As we know, cutter deformation and runout effect the machined surface quality, which make the actual machined surface deviate from the desired machined surface, and the deviation is defined surface error. The forming of surface error at $z_{i,j}$ is shown in Fig. 3. It is worth noting that the cutting traces of different flutes are not the same. A small area of the cutting trace is preserved around the "B" point ($\theta = \pi$), and other cutting traces will be cut by subsequent tooth and have no effect on the machined surface. "E" is a point in the small area, and its surface error can be given by

$$e_E(z_{i,j}) = \frac{D}{2} + R_{i,j}(\varphi)\cos\theta_{i,j}(\varphi) \tag{8}$$

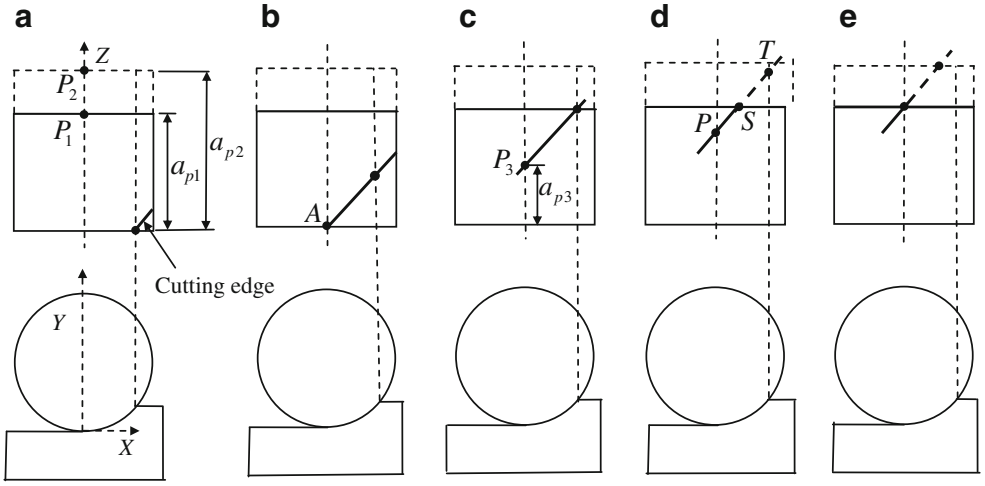

Fig. 4 Formation of machined surface in the two milling tests

Substituting Eqs. (6) to (8), the surface error can be simplified as

$$e_E(z_{i,j}) = -\rho\cos\left(\lambda - \frac{2z_{i,j}\tan\beta}{D} - \frac{2\pi(i-1)}{N}\right) + \delta_{yi,j}(\varphi) \quad (9)$$

Equation (9) shows that the surface error is mainly induced by runout and deformation in Y direction.

In real machining practice, several errors contribute to the final surface error, e.g., precision of machine tool, cutter runout and processing, etc. So, taking the total surface error as the cutter deformation is unreasonable. Also, it is difficult to identify the value of the cutting tool deformation component.

To obtain the cutter deformation from the surface error, two strips need to be machined with the same cutting conditions but with different axial depth only. The axial cutting depth a_p for the two milling tests are denoted as a_{p1} and a_{p2}, and are designed to meet Eq. (10) to ensure that there is only one tooth removing the material at any time, and the milling process is style I defined in reference [10].

$$\frac{D(\theta_{ex}-\theta_{st})}{2\tan\beta} < a_p < \frac{\left[\frac{2\pi}{N} - \arccos\left(1-\frac{2a_e}{D}\right)\right]D}{2\tan\beta} \quad (10)$$

Where, θ_{st} and θ_{ex} denote the start and exit radial immersion angles, respectively. a_e is radial cutting depth.

The mechanism of the surface forming for the two milling tests is shown in Fig. 4. Figure 4a demonstrates that the bottom segment of the cutting tool starts cutting. From this moment, other segments enter the cutting zone continuously. Until the bottom segment reaches the surface formation line as shown in Fig. 4b, the deformation and runout of the cutter does not contribute to the surface error. At this time, the milling forces and the cutter deformation are largest. Subsequently, the milling forces maintain the largest, but the cutter deformation decreases continuously because the cutting zone moves upward. Until the highest segment starts cutting in test 1(a_{p1}) as shown in Fig. 4c, the milling forces, the cutter deformation and machined surface in test 1 are same as them in test 2(a_{p2}) because the milling processes are similar. After this moment, segment between P_1 and P_2 start cutting, the milling forces in the two tests become different. Consequently, the surface and surface error are various till the tooth exit from the cutting zone in test 1 as shown in Fig. 4e.

As shown in Fig. 4c, when the highest segment starts cutting in test 1, the point P_3 is formed. The distance from the cutter bottom to the point is denoted as a_{p3} and calculated by

$$a_{p3} = a_{p1} - \frac{D(\theta_{ex}-\theta_{st})}{2\tan\beta} \quad (11)$$

The surface errors between P_3 and P_1 are different because the milling forces are various when the machined surfaces are formed in the two tests. As shown in Fig. 4d, when the point P is formed, the difference of the surface error is expressed by

$$\begin{aligned}\Delta e_P(z_{i,j}) &= e_P(z_{i,j})^{(2)} - e_P(z_{i,j})^{(1)} \\ &= \delta_{yi,j}(\varphi)^{(2)} + \varepsilon^{(2)} - \delta_{yi,j}(\varphi)^{(1)} - \varepsilon^{(1)}\end{aligned} \quad (12)$$

Where, $\Delta e_P(z_{i,j})$ denotes the difference of the surface error for the two tests. $e_P(z_{i,j})^{(1)}$ and $e_P(z_{i,j})^{(2)}$ represent the surface

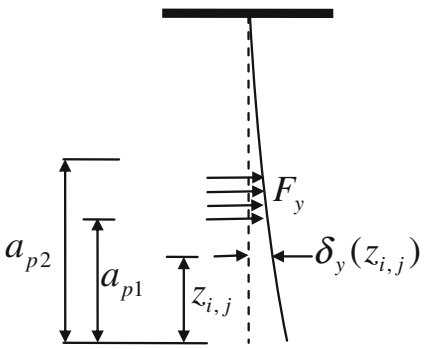

Fig. 5 Cutter deformation and milling force

Table 1 Feed per tooth for all the milling tests

Test	f_z/mm/r	Test	f_z/mm/r	Test	f_z/mm/r	Test	f_z/mm/r
1-1/2-1	0.01	1-4/2-4	0.04	1-7/2-7	0.07	1-10/2-10	0.1
1-2/2-2	0.02	1-5/2-5	0.05	1-8/2-8	0.08	1-11/2-11	0.11
1-3/2-3	0.03	1-6/2-6	0.06	1-9/2-9	0.09	1-12/2-11	0.12

error in tests 1 and 2, respectively. $\delta_{yi,j}(\varphi)^{(1)}$ and $\delta_{yi,j}(\varphi)^{(2)}$ are the cutter deformations when the point P is formed in test 1 and test 2. $\varepsilon^{(1)}$ and $\varepsilon^{(2)}$ are the errors induced by other factors except the cutter deformation in the two tests.

Because the two milling tests are done with the same cutting conditions except the axial depth, let $\varepsilon^{(1)} = \varepsilon^{(2)}$. According to the superposition principle of bending deformation for beam, which describes that deformation of the beam under several loads is equal to the sum of the several deformations induced by each load when the deformation is accord with Hooke law, Eq. (12) can be simplified as

$$\begin{aligned}\Delta e_P(z_{i,j}) &= \delta_{yi,j}(\varphi)^{(2)} - \delta_{yi,j}(\varphi)^{(1)} \\ &= \delta_{yi,j}(\varphi)^{(PS)} + \delta_{yi,j}(\varphi)^{(ST)} - \delta_{yi,j}(\varphi)^{(PS)} \\ &= \delta_{yi,j}(\varphi)^{(ST)}\end{aligned} \tag{13}$$

Where, $\delta_{yi,j}(\varphi)^{(ST)}$ and $\delta_{yi,j}(\varphi)^{(PS)}$ are the cutter deformations in Y direction induced by the milling forces generated by ST segment and PS segment.

Equation (12) shows that the difference of the surface errors in two milling tests is mainly caused by the cutter deformation induced by ST segment milling force as shown in Fig. 5. Once the surface errors are measured, the deformation will be obtained conveniently.

4 Calibration of instantaneous cutting force coefficients

When the machined surface point B_i is formed at the $z_{i,j}$ in the Z direction, the angular position of the tool $\varphi_{Bi}(z_{i,j})$ is

$$\varphi_{B_i}(z_{i,j}) = \pi + \frac{2z_{i,j}\tan\beta}{D} + \frac{2\pi(i-1)}{N} \tag{14}$$

In this case, the maximum axial height of the ST segment shown in Fig. 4d is $z_{\max} = z_{i,j} + D(\theta_{ex} - \theta_{st})/(2\tan\beta)$, and the minimum is $z_{\min} = a_{p1}$. So, the milling force induced by ST segment in Y direction is expressed as

$$F_y(\varphi') = \sum_{k=M1+1}^{M2} \left[K_T \sin\theta_{i,k}(\varphi') - K_R \cos\theta_{i,k}(\varphi')\right] h_{i,k}(\varphi') dz \tag{15}$$

Where, $M1 = z_{\min}/dz \cdot M2 = z_{\max}/dz \cdot \varphi' = \varphi_{B_i}(z_{i,j})$.

When other teeth are generating the surface points, all the tool teeth will exchange angular position successively. Due to the runout, when different tooth is forming the surface at the same axial height, the milling forces are various accordingly. However, the author has confirmed that runout has no effect on the nominal milling forces, and cutter deformation has little effect on the instantaneous chip thickness and only changes the boundary of cutting zone during steady milling in reference [20]. Thus, the nominal milling force induced by ST segment in Y direction can be given as

$$\overline{F_y(\varphi')} = \sum_{k=M1+1}^{M2} \left[K_T \sin\theta_{1,k}(\varphi) - K_R \cos\theta_{1,k}(\varphi)\right] f_z \sin\theta_{1,k}(\varphi) dz \tag{16}$$

Where, $\varphi = \pi + \frac{2z_{i,j}\tan\beta}{D}$.

According to the relation between milling force and cutter deformation, the cutter deformation corresponding with final machined surface points at the axial height $z_{i,j}$ will fluctuate periodically. Within a period of rotation, the peaks are denoted as $\delta_{yB_i}(z_{i,j})$, and the corresponding milling forces are expressed as $F_y(\varphi_{B_i}(z_{i,j}))$. Substituting Eqs. (16) to (5), the following equation can be obtained.

$$\begin{bmatrix} A & B \end{bmatrix} \begin{bmatrix} K_T \\ K_R \end{bmatrix} = \frac{1}{N} \sum_{i=1}^{N} \frac{\delta_{yB_i}(z_{i,j})}{A(z_{i,j})} \tag{17}$$

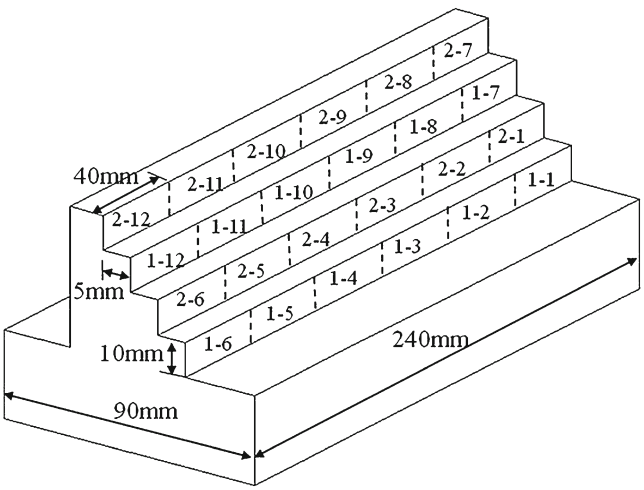

Fig. 6 Workpiece

Table 2 Cutting force coefficients and chip thickness

f_z/mm/r	$\overline{h}$/mm	K_T/N/mm^2	K_R/N/mm^2	f_z/mm/r	$\overline{h}$/mm	K_T/N/mm^2	K_R/N/mm^2
0.01	0.0048	5,241	4,075	0.07	0.0335	2,394	1,799
0.02	0.0096	3,614	3,239	0.08	0.0383	2,271	1,695
0.03	0.0144	3,337	2,721	0.09	0.0431	2,168	1,608
0.04	0.0191	3,186	2,111	0.10	0.0479	2,080	1,534
0.05	0.0239	2,834	2,091	0.11	0.0526	2,005	1,472
0.06	0.0287	2,444	1,927	0.12	0.0574	1,937	1,415

Where, $A = f_z \sum_{k=M1+1}^{M2} \sin\theta_{1,k}(\varphi)\sin\theta_{1,k}(\varphi)dz$. $B = -f_z \sum_{k=M1+1}^{M2} \cos\theta_{1,k}(\varphi)\sin\theta_{1,k}(\varphi)dz$.

$$A(z_{i,j}) = \frac{-(L-L_t)^3 + 3(L-L_t)^2(L-Z_F)}{6EI_t} + \frac{\langle Z_F - z_{i,j}\rangle^3 - (L_t - z_{i,j})^3 + 3(L_t - z_{i,j})^2(L_t - Z_F)}{6EI_t} + \frac{\left[-(L-L_t)^2 + 2(L-L_t)(L-Z_F)\right](L_t - z_{i,j})}{2EI_s}.$$

Equation (17) shows the relationship between the cutting coefficients and the surface errors at the certain axial height. It is necessary to measure surface errors at different axial heights to gather the different cutter deformations. Thus, Eq. (17) is extended to

$$\begin{bmatrix} A_1 & B_1 \\ A_2 & B_2 \\ \cdots\cdots & \\ A_n & B_n \end{bmatrix} \begin{bmatrix} K_T \\ K_R \end{bmatrix} = \begin{bmatrix} \frac{1}{N}\sum_{i=1}^{N}\frac{\delta_{yB_i}(z_1)}{A(z_1)} \\ \frac{1}{N}\sum_{i=1}^{N}\frac{\delta_{yB_i}(z_2)}{A(z_2)} \\ \cdots\cdots \\ \frac{1}{N}\sum_{i=1}^{N}\frac{\delta_{yB_i}(z_n)}{A(z_n)} \end{bmatrix} \quad (18)$$

Obviously, it is easy to calibrate the cutting force coefficients with the least squares method according to Eq. (18). To build the relationship between the coefficients and chip thickness as shown in Eq. (2), it is necessary to obtain the chip thickness. When the machined surface are formed at the axial height z_1 and z_n, the angular positions of the tool are $\varphi_1 = \pi + 2z_1\tan\beta/D$ and $\varphi_n = \pi + 2z_n\tan\beta/D$, respectively. It is worth noting that the coefficients deduced from Eq. (18) are average coefficients in the process. So, the chip thickness must be the average thickness of ST segment during the process, and can be calculated by

$$\overline{h} = \frac{D}{2(z_n - z_1)\tan\beta}\int_{\varphi_1}^{\varphi_n} \frac{\sum_{k=M1+1}^{M2} f_z \sin\theta_{1,k}(\varphi)dz}{\frac{D(\varphi-\theta_{st})}{2\tan\beta} - a_{p1}} d\varphi \quad (19)$$

Changing the feed per tooth for tests 1 and 2, several pairs of data including average cutting force coefficients and average chip thickness can be obtained and used to regression analysis to calibrate the instantaneous cutting force coefficients. Furthermore, the runout can be identified by iterative method presented in reference [11], with the best fit between theoretical and measured surface error as the criterion.

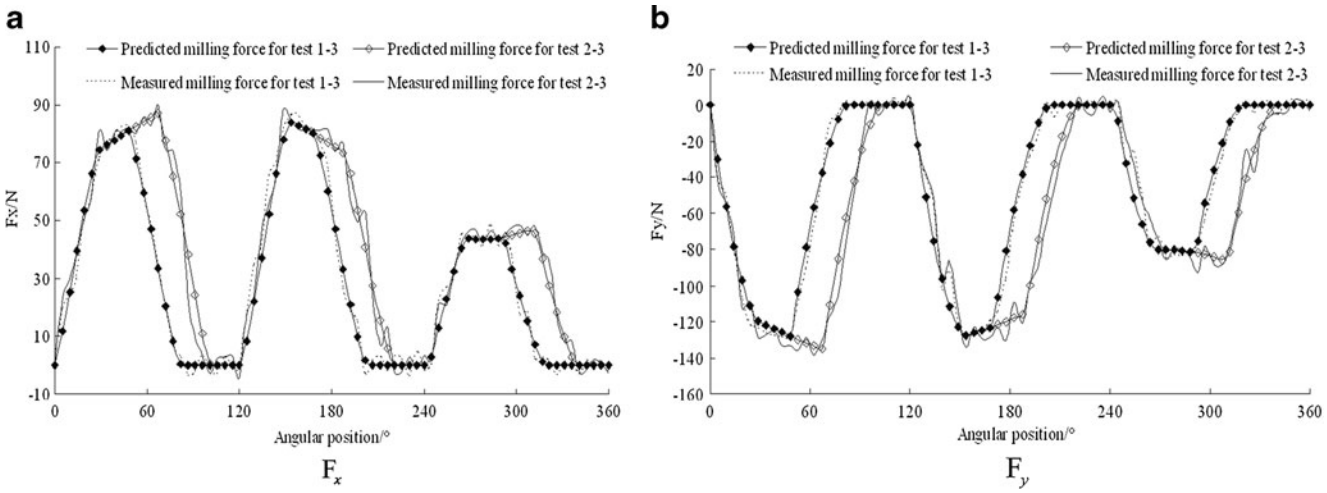

Fig. 7 Comparison of measured milling forces and predicted milling forces

Table 3 Comparison of predicted results with different method

		Measured results/N	Predicted results1		Predicted results 2	
			Results/N	Relative error (%)	Results/N	Relative error (%)
Average of test 1-3	F_x	28.5	27.8	2.46	29.8	4.56
	F_y	47.2	45.2	4.23	49.5	4.87
Maximum of test 1-3	F_x	85.4	84	1.65	89.5	4.8
	F_y	130.4	127.8	1.99	143.9	10.35
Average of test 2-3	F_x	39.3	38.8	1.30	40.7	3.56
	F_y	63.5	62.8	1.10	69.3	9.13
Maximum of test 2-3	F_x	86	84	2.33	92.5	7.52
	F_y	142.3	135.1	5.06	156	9.65

5 Experimental verifications

Now, a series of milling tests are carried out on milling machine with good rigidity to determine instantaneous cutting force coefficients and runout parameters. A HSS 3-flute 12 mm flat end cutter with 45° helix angle is used, which has 110 mm total length, 45 mm flute length, and 83 mm overhang length. The modulus of elasticity for the cutter is 206 GPa. The material of test piece is Al6061-T6. Surface errors are measured by a coordinate measuring machine MISTRAL-775 and milling forces are measured by a force meter Kistler9257B.

The conditions for all the milling tests are spindle speed n=3,000 r/min, radial depth a_e=1 mm, dry cutting and down milling. The axial depths for tests 1-1~1-12 and tests 2-1~2-12 are 5 and 7 mm, respectively. The feed per tooth for the milling tests are listed in Table 1.

To eliminate the surface error induced by clamping workpiece and tool setting, all milling tests and pretreatment are carried out with the same operational datum by one tool setting on the same workpiece. The workpiece is shown in Fig. 6 and accommodates four strips which divided into six sections.

Because machined surface formed by test 1-i and test 2-i become different at the axial height a_{p3}, and milling forces generated by ST segment is largest when the surface at the axial height $\min\{a_{p1}, a_{p2} - D(\theta_{ex} - \theta_{st})/2\tan\beta\}$ is formed. So, the surface between 1.486 and 3.486 mm in all tests are measured to be used to determine the cutting force coefficients. Measuring tool path are straight with 0.2 mm step increment in Z direction and $f_z/4$ step increment in X direction.

According to Eq. (13), cutter deformations are obtained. Further, cutting force coefficients and chip thickness are calculated with Eqs. (18) and (19). The results are listed in Table 2, from which it can be seen that the cutting force coefficients have the tendency to vary dramatically and to become large when chip thickness becomes small. The fitting functions from the experimental data are

$$\begin{cases} K_t(h) = 629.27h^{-0.3934} \\ K_r(h) = 396.38h^{-0.4454} \end{cases} \tag{20}$$

Runout parameters can be estimated by iterative method with good prediction accuracy, and the results are ρ=2.2 μm and λ=109°.

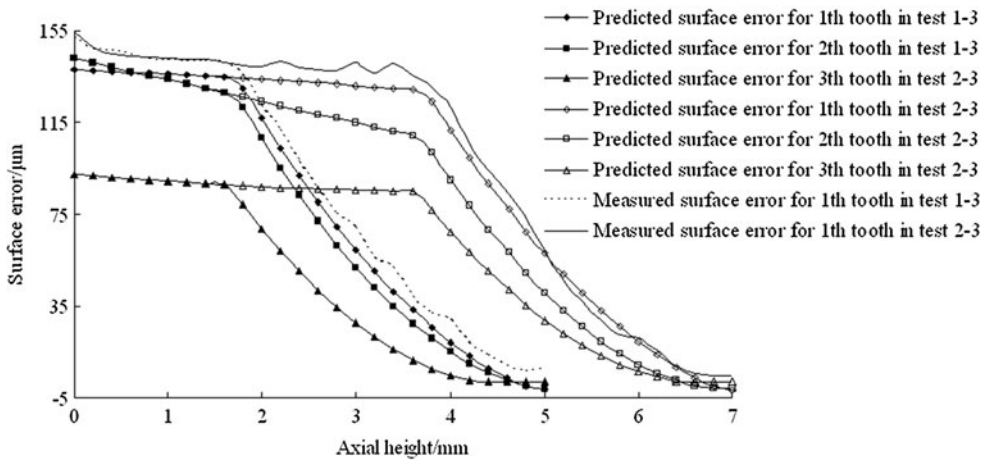

Fig. 8 Comparison of measured surface errors and predicted surface errors

The estimated instantaneous cutting force coefficients and runout parameters are used to predict the milling force for tests 1–3 and 2–3. The predicted forces and measured forces are given in Fig. (7). Obviously, the predicted milling forces are in good agreement with measured forces both in *X*- and *Y*-direction. It proves the validity and accuracy of the cutting force coefficients and runout parameters obtained with the presented method. Also, milling forces are predicted with other method, and the predicted results are compared in Table 3. Predicted results 1 are obtained with the method proposed in the paper. Predicted results 2 are obtained with the method presented in reference [11]. It can be seen from Table 3 that more accurate estimate of milling forces can be obtained with the new method.

In practice, cutter deformation, milling forces and cutting zone have interaction. Neglecting cutting chatter, a balance will be achieved between cutter deformation and milling forces. In this case, the cutter deformation will be recorded on the machined surface. So, it is necessary to determine the balance state when surface errors are predicted considering cutter deformation. Iterative corrections of radial cutting depth presented in reference [21] are adopted to determine the balance state. According to Eq. (9), surface errors for tests 1–3 and 2–3 are predicted and shown in Fig. 8. The predicted results are in agreement with the measured results, and the maximum relative deviation is 12 %. All these indicate that calibrated cutting force coefficients and runout parameters are accurate, and the prediction method of surface error is validated.

Also, it can be seen that although the runout is only 2.2 μm, the surface errors induced by the three teeth are different significantly. So, effect of runout on surface error is not negligible. The surface errors for the two tests are almost same under the axial height 1.6 mm in measured results and predicted results, but different up the axial height 1.6 mm due to the different milling forces. As shown in Fig. 9, the difference between predicted results of tests 1–3 and predicted results of tests 2–3 is consistent with the difference between measured results of tests 1–3 and measured results of tests 2–3. Because other effect facts are eliminated by difference method, the difference is cutter deformation only.

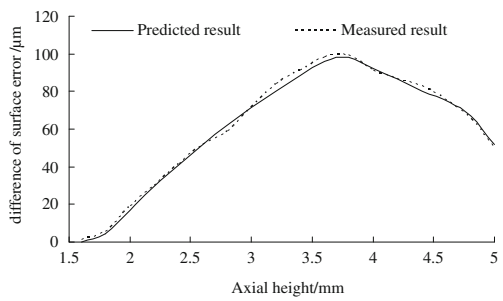

Fig. 9 Difference of predicted and measured surface error for 1th tooth

Although runout does not affect the dynamic behavior of the milling process according the chatter boundaries, it has a strong influence on the vibration trajectory of the milling tool and on the resulting surface quality. Particularly, when cutting parameters are minimum values, the effect is more significant, and radial runout of the cutter can disrupt the measured signal. Figure 9 shows that the difference method can eliminate the effect of radial runout and calibrate the cutter deformation.

To validate the method, experiments are carried out under the same conditions with Sandvik R216.34-10030-AS14N1630 tool. The cutting force coefficients are calibrated as

$$\begin{cases} K_t(h) = 219.26h^{-0.4907} \\ K_r(h) = 13.477h^{-0.905} \end{cases} \tag{21}$$

Calibrated runout parameters are ρ=8.1 μm and λ=101°. With the calibrated parameters, milling forces are predicted in Fig. 10, also the experiment is carried out. The cutting parameters are feed rate f_z=0.025 mm/tooth, spindle speed n =4000 r/min, axial depth a_p=1.5 mm and radial depth a_e= 2.5 mm. Figure 10 shows that the simulated results are in agreement with the measured results, that means the proposed method is effective similarly when large stiffness cutter is used.

6 Conclusions

A new approach is proposed to calibrate the instantaneous cutting force coefficients and runout parameters in flat end milling. Firstly, a milling force model and a surface error model are presented. With the surface model, cutter deformation can be estimated by two tests which have the same cutting conditions but different axial depth only, and also be expressed by the surface errors formed in the two tests.

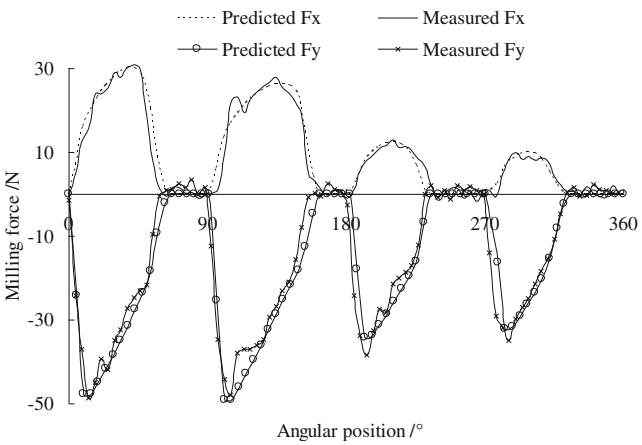

Fig. 10 Comparison of the simulated and measured results for other cutting parameters

Further, according to the relationship between the cutter deformation and milling force, relationships between the surface errors and the cutting force coefficients are proposed. Thus, identification method of instantaneous cutting force coefficients using surface errors is presented. Finally, the proposed approach is tested with a series of milling tests and validated by comparing the predicted results and experimental results. The main advantage of the approach is that it significantly reduces the effect of the errors that appear during the machining because cutting force coefficients are calculated by resultant cutter deformation instead of the absolute surface error. Also, it does not require expensive force meter in practice.

Acknowledgments The work is supported by the natural science foundation of the Jiangsu Province of China (BK2012476) and scientific foundation of Nanjing institute of technology (ZKJ201201).

References

1. Kline WA, DeVor RE, Lindberg JR (1982) The prediction of cutting forces in end milling with application to cornering cuts. Int J Mach Tool Manuf 22:7–22
2. Altintas Y, Spence A (1991) End milling force algorithms for CAD systems. Ann CIRP 40:31–34
3. Gradusek J, Kalveram M, Weinert K (2004) Mechanistic identification of specific force coefficients for a general end milling. Int J Mach Tool Manuf 44:401–414
4. Kuo CP, Ling CC, Chen SH (2006) The prediction of cutting force in milling inconel-718. Int J Adv Manuf Technol 27:655–660
5. Kang YG, Wang ZQ, Wu JJ, Jiang CY (2007) Study of the classification of cutting forces and the build of the accurate milling force model in end milling. Acta Aeronaut Astronaut Sin 28 (2):481–489, in Chinese
6. Liu M, Jing LL, An QL, Chen M (2009) Study on cutting force coefficients in end milling die steel 4Cr16MO. J Shanghai Jiaotong Univ 43(1):25–29, in Chinese
7. Yun WS, Cho DW (2000) An improved method for the determination of 3D cutting force coefficients and runout parameters in end milling. Int J Adv Manuf Technol 16:851–858
8. Ko JH, Cho DW (2005) Determination of cutting condition independent coefficients and runout parameters in ball-end milling. Int J Adv Manuf Technol 26:1211–1221
9. Azeem A, Feng HY, Wang L (2004) Simplified and efficient calibration of a mechanistic cutting force model for ball-end milling. Int J Mach Tool Manuf 44:291–298
10. Bhattacharyya A, Schueller JK, Mann BP, Ziegert JC, Schmitz TL, Taylor FJ, Fitz-Coy NG (2010) A closed form mechanistic cutting force model for helical peripheral milling of ductile metallic alloys. Int J Mach Tool Manuf 50:538–551
11. Wan M, Zhang WH, Qin GH, Tan G (2007) Efficient calibration of instantaneous cutting force coefficients and runout parameters for general end mills. Int J Mach Tool Manuf 47:1767–1776
12. Wan M, Zhang WH, Qin GH, Wang ZP (2008) Consistency study on three cutting force modeling methods for peripheral milling. Proc IMechE B 222:665–676
13. Rivière-Lorphèvre E, Filippi E (2009) Mechanistic cutting force model parameters evaluation in milling taking cutter radial runout into account. Int J Adv Manuf Technol 40:12–25
14. Franco P, Estrems M, Faura F (2004) Influence of radial and axial runouts on surface roughness in face milling with round insert cutting tools. Int J Mach Tool Manuf 44:1555–1565
15. Salgado MA, Lopez de Lacalle LN, Lamikiz A, Munoa J, Sanchez JA (2005) Evaluation of the stiffness chain on the deflection of end-mills under cutting forces. Int J Mach Tool Manuf 45:727–739
16. Siller HR, Vila C, Rodriguez CA, Abellan JV (2009) Study of face milling of hardened AISI D3 steel with a special design of carbide tools. Int J Adv Manuf Technol 40:12–25
17. Kim GM, Kim BH, Chu CN (2003) Estimation of cutter deflection and form error in ball-end milling. Int J Mach Tool Manuf 43:917–924
18. Xu AP, Qu YX, Zhang DW, Huang T (2003) Simulation and experimental investigation of the end milling process considering the cutter flexibility. Int J Mach Tool Manuf 43:283–292
19. Dotcheva M, Millward H, Lewis A (2008) The evaluation of cutting-force coefficients using surface error measurements. J Mater Process Technol 196:42–51
20. Wang BS (2011) Parameters identification of instantaneous milling force model and its experimental investigation. Jiangsu University, Zhenjiang, in Chinese
21. Wan M, Zhang WH (2006) Efficient algorithms for calculations of static form errors in peripheral milling. J Mater Process Technol 171:156–165